Article

Cell Reports

Overproduction of Neurons Is Correlated with Enhanced Cortical Ensembles and Increased Perceptual Discrimination

Graphical Abstract

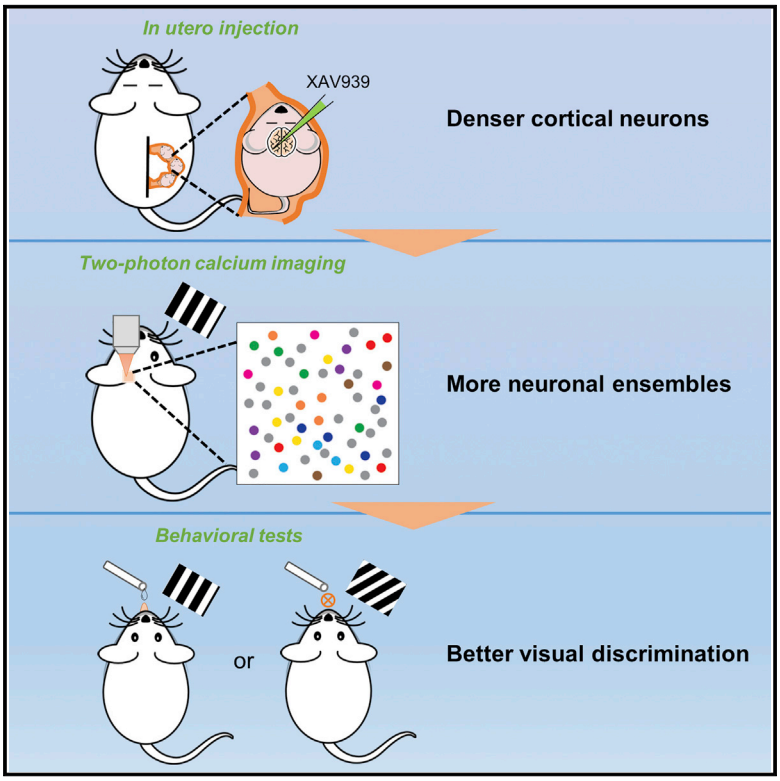

Authors

Wei-Qun Fang, Rafael Yuste

Correspondence

wf2203@columbia.edu

In Brief

Fang et al. report that mice engineered to have more cortical neurons also have more neuronal ensembles and improved visual discrimination compared to wild-type mice. These findings suggest that neuronal production is linked to functional modularity and perceptual discrimination in the visual cortex.

Highlights

- In utero XAV939 injections lead to neuronal overproduction
- XAV939 injections strengthen functional correlations among V1 neurons
- XAV939 injections increase neuronal ensemble number and segregation
- XAV939-injected mice have sharper orientation discrimination

Fang & Yuste, 2017, Cell Reports *21*, 381–392
October 10, 2017
https://doi.org/10.1016/j.celrep.2017.09.040

CellPress

Cell Reports
Article

Overproduction of Neurons Is Correlated with Enhanced Cortical Ensembles and Increased Perceptual Discrimination

Wei-Qun Fang[1,2,*] and Rafael Yuste[1]
[1]Neurotechnology Center, Department of Biological Sciences, Columbia University, New York, NY 10027, USA
[2]Lead Contact
*Correspondence: wf2203@columbia.edu
https://doi.org/10.1016/j.celrep.2017.09.040

SUMMARY

Brains vary greatly in neuronal number and density, even across individuals within the same species, yet it remains unclear whether such variation leads to differences in brain function or behavior. By imaging cortical activity of a mouse model in which neuronal production is moderately enhanced in utero, we find that animals with more cortical neurons also develop enhanced functional correlations and more distinct neuronal ensembles in primary visual cortex. These mice also have sharper orientation discrimination in their visual behavior. These results unveil a correlation between neuronal ensembles and behavior and suggest that neuronal number is linked to functional modularity and perceptual discrimination of visual cortex. By experimentally linking differences in neuronal number and behavior, our findings could help explain how evolutionary and developmental variability of individual and species brain size may lead to perceptual and cognitive differences.

INTRODUCTION

What make human brains special? Could their larger size account for more advanced cognitive abilities? In both mammalian and avian brains, larger neuronal density and number are correlated with increased perception and mental abilities (Herculano-Houzel et al., 2014; Olkowicz et al., 2016; Roth and Dicke, 2005). Moreover, variations in neuronal density not only occur across cortical areas in the same species (Collins et al., 2010) but also within the same cortical region among individuals (Herculano-Houzel, 2009). The intraspecific variability in neuronal number probably influences the structural and functional basis of neural circuits, leading to differences in brain function and behavior (Mueller et al., 2013; Song et al., 2013; Vogel and Machizawa, 2004; Ward et al., 1998). Despite this, few studies have tested experimentally how the number of neurons or neuronal density influence brain function and behavior. Moreover, a causal link between neuronal number and brain function at the neural circuit level has not been directly explored. To test this, an ideal experiment would be to manipulate neuronal number and subsequently quantify the properties of neural circuits of simple brain functions, preferably those related to innate behaviors, to avoid confounding factors such as environmental influences or learning.

The manipulation of neuronal number can be achieved by regulating intrinsic and extrinsic factors that alter neuron production or cell death (Williams and Herrup, 1988). But to interpret these manipulations, it is critical to minimize the influence of genetic background, experience, and environment. To this end, we investigated a mouse model in which the neurogenesis rate of excitatory neurons can be pharmacologically modulated (Fang et al., 2014) through in utero injection of the chemical compound XAV939 (XAV) into the lateral ventricle of the developing cortex at embryonic day (E) 14.5. XAV939 penetrates the neural progenitor cells and prevents Axin degradation, and this transiently accelerates the proliferation of neural progenitors and moderately increases the production of pyramidal neurons in neocortical layer 2/3 (Fang et al., 2013, 2014). In addition, these mice exhibit abnormal dendritic arborization, synaptic connections, and cortical activity, as well as atypical behaviors (Fang et al., 2014), suggesting that altered neural circuitry and function could arise from neuronal overproduction.

Because the orientation preference of neurons in the primary visual cortex (V1) emerges mostly independently of visual experience (Hubel and Wiesel, 1959; White and Fitzpatrick, 2007), we chose orientation discrimination in V1 as an assay to study how prenatal variation in brain development regulates neural circuit function and behavior. To quantify cortical function at the circuit level, we measured the activity of neuronal populations in V1 with two-photon calcium imaging (Stosiek et al., 2003; Yuste and Katz, 1991) and analyzed neuronal ensembles (or assemblies), which are coactive groups of neurons that coordinate their activities and could represent distinct cognitive entities (Harris et al., 2003; Hebb, 1949). Neuronal ensembles spontaneously exhibit coherent activity (Cossart et al., 2003; Harris, 2005; Ikegaya et al., 2004; Lampl et al., 1999) that mimics stimulus-evoked activity patterns (Kenet et al., 2003; Luczak et al., 2009; MacLean et al., 2005; Miller et al., 2014) and can be optogenetically imprinted into cortical circuits (Carrillo-Reid et al., 2016). Because of these properties, they have been proposed to be basic circuit building modules of neural circuits (Harris et al., 2003; Yuste, 2015). Because neuronal ensembles likely arise from recurrent neuronal connectivity (Sanchez-Vives and McCormick, 2000), changes in neuronal connectivity due to

neuronal overproduction (Fang et al., 2014) may affect the organization and function of neuronal ensembles.

Here, we investigated how neuronal production regulated neuronal ensembles and orientation discrimination in V1 using the XAV939-injection mouse model. We generated mice with higher densities of layer 2/3 neurons and performed two-photon in vivo calcium imaging to measure their spontaneous and visually evoked activity. We find that XAV939-injected animals develop stronger functional correlations among neurons and generate more functionally clustered neuronal ensembles. Moreover, we find that XAV939-treated mice have sharper orientation discrimination. Our work thus demonstrates that neuronal production level can shape the functional modularity of the neocortex and regulate perceptual discrimination of animals. This study also uncovers a correlation between number of neuronal ensembles and perceptual discrimination, strengthening the case for their functional role in cortical function.

RESULTS

Neuronal Overproduction Induced by XAV939 Injections Strengthens Neuronal Pairwise Correlations

In our previous work using post-mortem fixed tissue, we showed that in utero injection of XAV939 into the lateral ventricle of developing cortex at E14.5 generated mice with additional neurons in cortical layer 2/3, without altering neuron size (Fang et al., 2014). Now, we replicated these findings in living mice to perform functional studies in vivo. Layer 2/3 neurons in V1 of adult mice were bulk loaded with a synthetic calcium indicator Oregon Green Bapta-1 acetoxymethyl (AM) (OGB1) (Figures 1A and 1B; Movie S1), which ubiquitously labels neurons (Stosiek et al., 2003). Larger numbers of OGB1-positive neurons were found in the visual cortex of XAV939-treated animals (186 ± 11 cells within 250 × 250 μm^2 regions; mean ± SEM; n = 6 mice) than in that of control animals (154 ± 9 within 250 × 250 μm^2 regions; mean ± SEM; n = 7 mice) ($p = 0.0415$; Student's t test) (Figure 1C), confirming that in utero XAV939 injection leads to neuronal overproduction (Fang et al., 2014).

Because neuronal overproduction altered synaptic connections in post-mortem fixed cortical tissues (Fang et al., 2014), we first tested whether it also affected functional selectivity and connectivity of neurons. To image the activity of neuronal populations for longer periods, neurons were labeled with the genetically encoded calcium indicator GCaMP6s under the neuron-specific human synapsin promoter (Figures 1A and 1D; Movie S2) (Chen et al., 2013). With two-photon in vivo calcium imaging of GCaMP6s-active neurons in layer 2/3 of V1 of adult XAV939-treated and control animals (postnatal day [P] 60–65), we measured the spontaneous activity in the dark and the visually evoked responses to oriented drifting gratings. From the time course of GCaMP6s fluorescent ΔF/F signals (Figure 1E), we inferred calcium spiking events (Figure 1F) using constrained nonnegative deconvolution algorithms (Pnevmatikakis et al., 2016; Yang et al., 2016) and reconstructed the spatiotemporal spiking activity of the local neural network (Figure 1G). The activity of the whole neuronal population, revealed by the sum of all spiking events, was similar in control and XAV939 brains (spontaneous activity, n = 12 control [CON] and n = 10 XAV939 mice; evoked activity, n = 7 control and n = 7 XAV939 mice) (Figure 1H). Moreover, XAV939 treatment did not substantially alter the functional properties of individual neurons, e.g., orientation or direction selectivity (n = 7 control and n = 7 XAV939 mice) (Figures 1I and S1A–S1C), orientation preference (Figures S1D and S1E), and the intermixed distribution of orientation-selective neurons (Figures S1F and S1G). Nonetheless, although pairwise correlations of individual neurons were weak overall, because most pairwise correlation coefficients (control, 62.9 ± 3.1%; XAV939, 54.9 ± 3.8%; mean ± SEM) were smaller than 0.01, neuronal correlations were stronger in XAV939 brains during both spontaneous and evoked activities (Figure 1J), implying that animals with increased neurons also have stronger local connectivity (Schneidman et al., 2006).

XAV939 Treatment Enhances Neuronal Group Coactivation in Spontaneous and Visually Evoked Activity

Alteration of functional correlations among neurons may influence their population coding and computation (Averbeck et al., 2006). We therefore investigated whether the joint activity of groups of neurons was affected in XAV939 mice. Coactive neurons were defined as those with spiking events in the same frame (250 ms/frame) (Figure 1G); thus, a binary vector was able to denote the coactivity of a group of neurons in each frame (Figure 2A) (Carrillo-Reid et al., 2016). In line with previous studies (Miller et al., 2014), most spiking events (61.7% ± 2.6%; mean ± SEM) occurred in a small proportion of frames (14.6% ± 0.7%; mean ± SEM), which exhibited statistically significant numbers of active neurons (Figures 2B, S2A, and S2B), previously defined as high-activity frames (Miller et al., 2014). Although XAV939 treatment did not substantially affect the number (Figure 2C) and neuronal coactivity level (Figure 2D) of high-activity frames, it elevated the correlation between pairs of high-activity frames, as shown by a higher cosine similarity (Figure 2E). Because most pairwise correlations (81.5% ± 0.7%; mean ± SEM) were weak (cosine similarity < 0.01), we focused on the statistically significantly correlated pairs (Figures 2F, S2C, and S2D) and measured their mutual correlation patterns (Figure 2G), which reflected the functional clustering of neuronal groups (Miller et al., 2014). High-activity frames in XAV939 brains were more mutually correlated, as shown by larger fraction of high-activity frames participating in the mutual correlation patterns (Figure 2H). Thus, coactivation of similar groups of neurons occurs more frequently in XAV939 brains.

XAV939 Treatment Increases the Number of Neuronal Ensembles in Spontaneous and Visually Evoked Activity

To further elucidate the functional clustering of neuronal groups, we investigated neuronal ensembles, which have been postulated to be basic circuit building blocks of the cortex and hippocampus (Harris et al., 2003; Feldt Muldoon et al., 2013; Yuste, 2015). Although ensembles can be mapped at various spatiotemporal precisions and named differently (e.g., assemblies, oscillations, reverberations, synfire chains, flashes, attractors, avalanches, songs, groups, clicks, or bumps), one of their most fundamental properties is the concurrent and recurrent firing of groups of neurons, forming an emergent functional unit. We

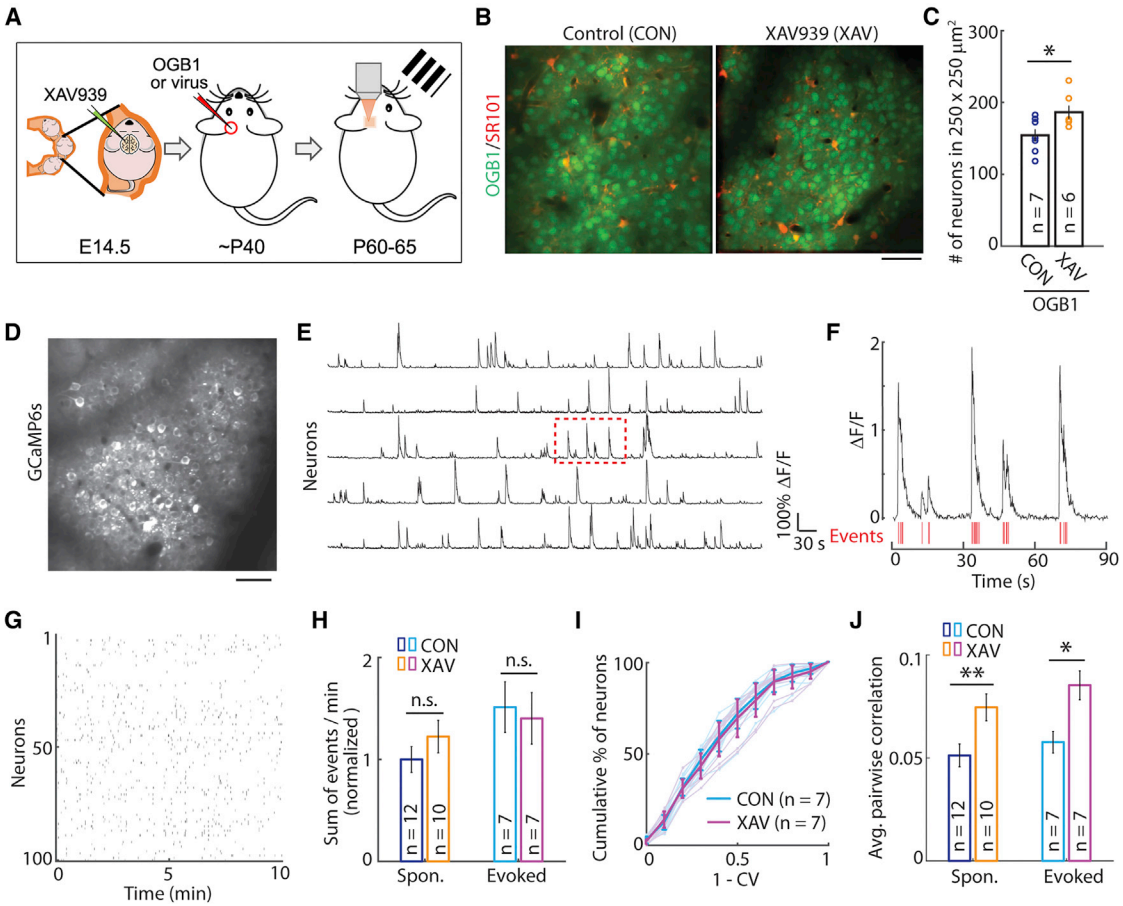

Figure 1. Neuronal Overproduction Induced by XAV939 Treatment Strengthens Neuronal Correlations

(A) Schematic of experimental workflow.

(B) In vivo two-photon calcium imaging of neurons that were labeled with OGB1 in layer 2/3 of monocular V1 at P40-45. Sulforhodamine 101 (SR101)-labeled astrocytes. Scale bar, 50 μm.

(C) XAV939 injection caused neuronal overproduction. Each circle denotes the average total number of neurons within 250 × 250 μm^2 regions in layer 2/3 of V1 of an animal. For each mouse, multiple (3–5) neighboring regions were imaged, and their average total number of neurons was represented as a circle. CON, control; XAV, XAV939 injected.

(D) An example of the GCaMP6s-labeled neuronal population. Due to the low baseline fluorescence, most GCaMP6s-positive neurons are barely visible in this image. Scale bar, 50 μm.

(E) Examples of fluorescent signals of active neurons. The signals within the dashed rectangle were amplified in (F).

(F) Spiking events were inferred from ΔF/F traces of fluorescent signals using the constrained non-negative deconvolution algorithms.

(G) An example of the time course spiking events of each neuron in a neuronal population. Each black dot represents a spiking event in a frame.

(H) Neuronal overproduction did not substantially alter the overall activity of neuronal populations. The average overall spontaneous activity of control brains was set as 1. Spon., spontaneous.

(I) Neuronal overproduction did not substantially alter the orientation selectivity of neuronal populations. Bold lines denote the average responses. Orientation selectivity of individual neurons was quantified by 1 − circular variance (1 − CV) of the normalized responses to orientations.

(J) Neuronal overproduction strengthened pairwise neuronal correlations in spontaneous and visually evoked activities. The level of correlation was determined by the Pearson correlation coefficients of spiking events of neurons.

Data are represented as mean ± SEM; *$p < 0.05$, **$p < 0.01$; n.s., not significant; Student's t test (C) or Wilcoxon rank-sum test (H and J). The n values represent the number of mice for each group or condition. See also Figure S1 and Movies S1 and S2.

therefore searched for sets of neurons that were repeatedly coactive in multiple mutually correlated high-activity frames (Figure 3A), previously defined as core ensembles (MacLean et al., 2005; Miller et al., 2014). In comparison to independent surrogate datasets, in which active neurons in each high-activity frame were permuted while the total number of spiking events of each neuron was preserved, we established that a repetition of 2 neurons in 2 frames was an adequate threshold for statistical significance (Figures 3B and 3C). Therefore, core ensembles (short as ensembles) in this study were defined as sets of common neurons (≥3 neurons) that repeatedly (≥3 high-activity frames) coactivated within a fixed time window (a frame, 250 ms). Based on these criteria, we identified spontaneous and visually evoked ensembles in the 320 × 320 μm^2 imaged

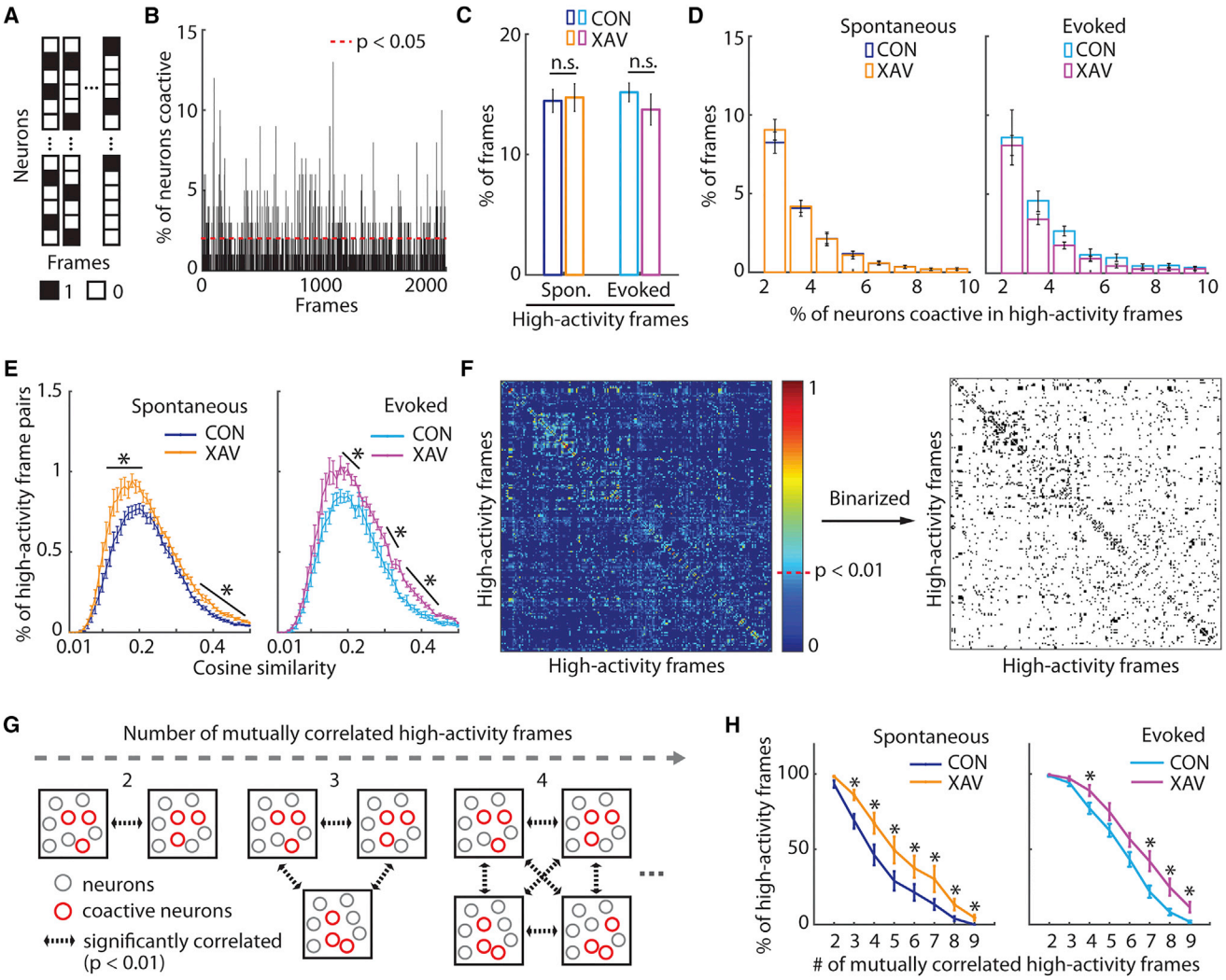

Figure 2. XAV939 Treatment Enhances Coactivation of Neuronal Groups

(A) Schematic of a binary matrix illustrating groups of coactive neurons in each frame. 1, active; 0, inactive.

(B) Varying degrees of neuronal coactivation in each frame. The red dashed line indicates the threshold for determining high-activity frames.

(C) XAV939 treatment did not significantly alter the proportion of high-activity frames.

(D) XAV939 treatment did not affect the distribution of neuronal coactivation in high-activity frames.

(E) XAV939 treatment elevated pairwise correlation between high-activity frames in spontaneous and visually evoked activities. The level of correlation was determined by cosine similarity of the binary vectors of frames shown in (A).

(F) An example of the identification of statistically significantly correlated high-activity frame pairs. The cosine similarity coefficients that passed the threshold were converted to 1 (correlated) and otherwise were 0 (uncorrelated).

(G) Schematic of sets of mutually correlated high-activity frames. High-activity frames in each set were statistically significantly correlated to each other ($p < 0.01$).

(H) Larger proportion of high-activity frames participated in the mutually correlated frame sets in XAV939 brains, indicating that increasing neuronal density enhanced the reverberation of neuronal coactivation.

Data are represented as mean ± SEM; *$p < 0.05$; n.s., not significant; Wilcoxon rank-sum test. See also Figure S2.

fields (Figure 3D). Spiking activities of neurons were highly correlated in the same spontaneous or evoked ensembles, but not in randomized neuron groups (Figure 3E), corroborating previous reports that ensembles are stable and likely arise from the structural and/or functional connections of cortical microcircuits (MacLean et al., 2005; Miller et al., 2014). Because XAV939 treatment regulated neuronal anatomical connections (Fang et al., 2014) and pairwise correlations (Figure 1I), we assessed how it affected ensembles. Although the number of neurons per ensemble was not larger in XAV939 mice (Figure 3F), the numbers of spontaneous and visually evoked ensembles were markedly increased (Figure 3G).

To confirm this result and overcome the variability caused by varying numbers of labeled neurons in different mice, we imaged multiple (3–5) neighboring regions in each mouse (Figure 4A), partitioned each into five 200 × 200 μm^2 subregions (Figure 4B),

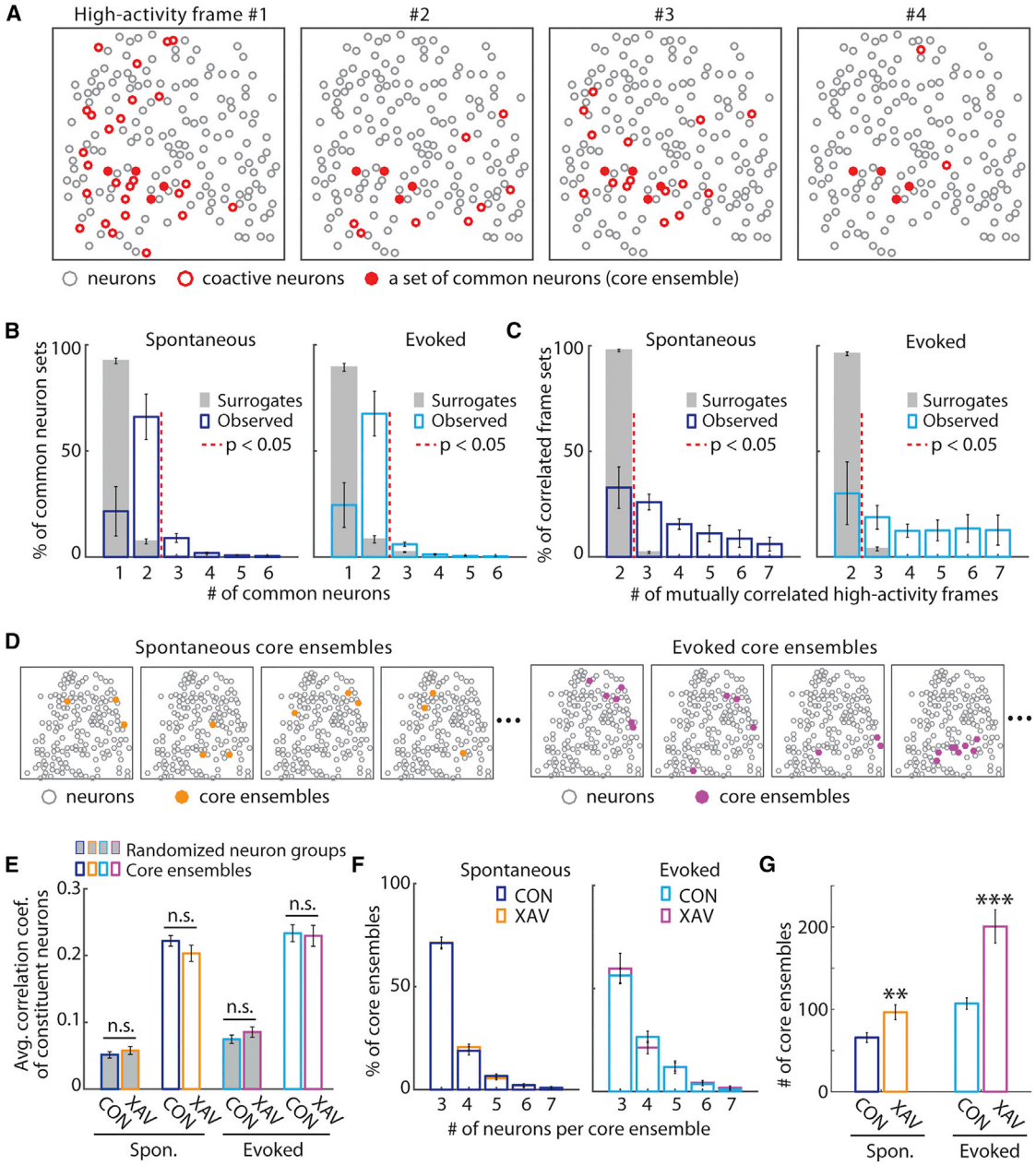

Figure 3. XAV939 Treatment Increases the Number of Stable Neuronal Ensembles

(A) Illustration of a set of common coactive neurons in several mutually correlated high-activity frames.

(B and C) The size thresholds of neuron (B) and frame (C) sets were statistically established as 2 common neurons and 2 high-activity frames. The thresholds were determined to be the values that were higher than 95% of the sizes of all neuron or frame sets identified from 5,000 independent surrogate datasets, in which the active neurons in each frame were shuffled while the total number of spiking events in each neuron was preserved.

(D) Spontaneous and visually evoked core ensembles were mapped. Core ensembles were defined as sets of common neurons ($\geq$3 cells) that repeatedly ($\geq$3 high-activity frames) coactivate within a fixed time window (a frame).

(E) Constituent neurons of the same spontaneous or evoked core ensembles were highly correlated in activity. Randomized neuron groups were simulated by randomly exchanging the constituent neurons of core ensembles while preserving the number and size of core ensembles, as well as the participation rate of each neuron in all core ensembles. Avg., average; coef., coefficient.

(F and G) XAV939 treatment did not affect the number of neurons per ensemble but increased the ensemble number. The fractions of core ensembles with varying sizes (F) and numbers of core ensembles (G) were summaries of core ensembles in 320 × 320 μm^2 imaged fields of 12 control mice (spontaneous and evoked activities of 43 and 16 imaged fields, respectively) and 10 XAV939-treated mice (spontaneous and evoked activities of 34 and 14 imaged fields, respectively). Data are represented as mean ± SEM; **p < 0.01, ***p < 0.001; n.s., not significant; Wilcoxon rank-sum test.

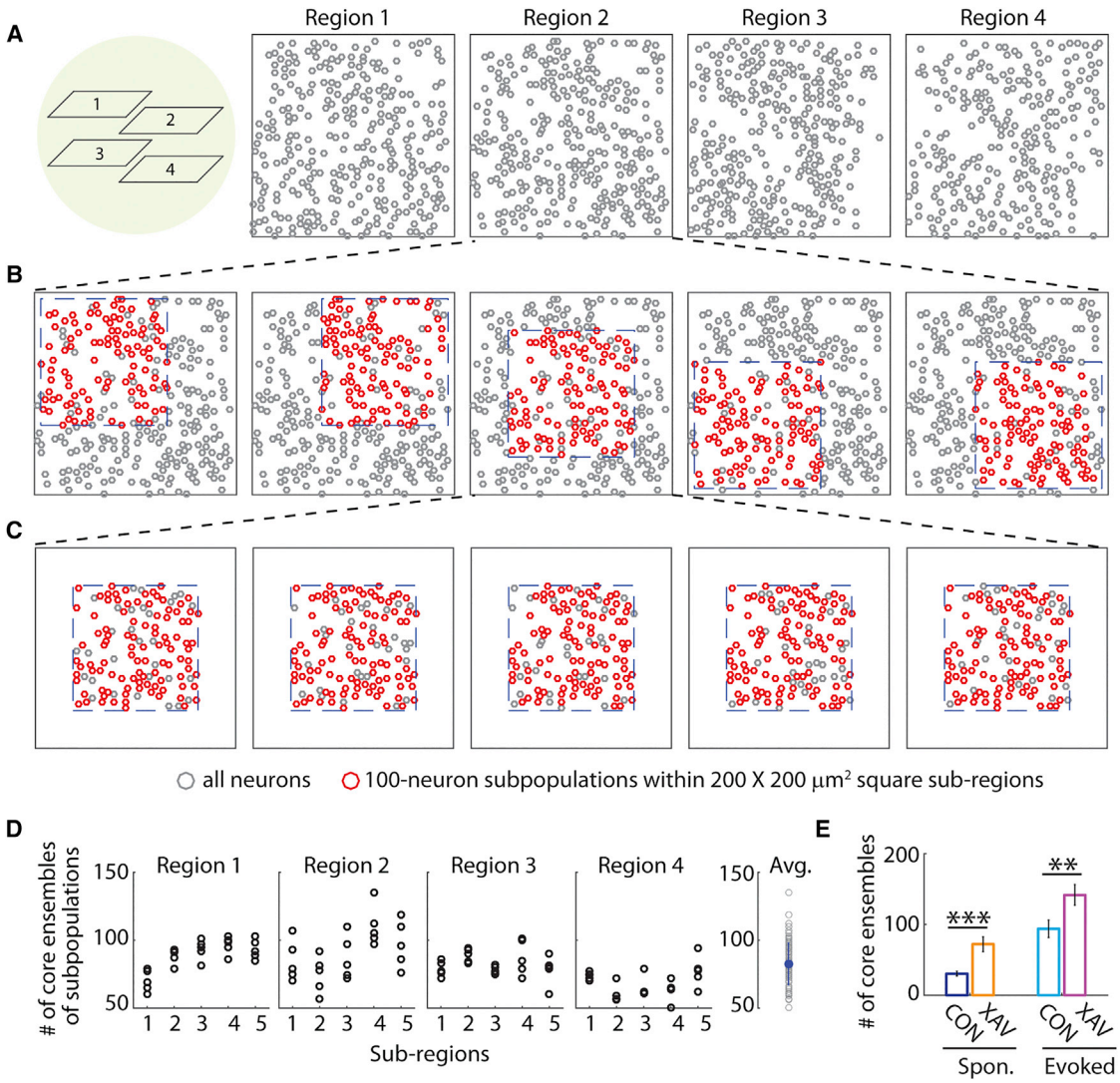

Figure 4. Neuronal Overproduction Increases the Rate of Ensemble Generation

(A) Illustration of 4 neighboring imaged regions in cortical layer 2/3 of V1 of a mouse.

(B and C) Schematic of partitioning the imaged neuronal population into multiple 100-neuron subpopulations (C) within 200 × 200 μm^2 subregions (B).

(D) Core ensemble numbers of all subpopulations of 4 neighboring imaging regions and their average value. Each open circle represents the core ensemble number in each 100-neuron subpopulation. The average value of the core ensemble number (blue dot) was used to represent the level of ensemble generation of the animal. Data are represented as mean ± SD.

(E) XAV939-treated brains generated more spontaneous and evoke core ensembles in the 100-neuron subpopulation.

Data are represented as mean ± SEM; **p < 0.01, ***p < 0.001; Wilcoxon rank-sum test.

and randomly picked five 100-cell subpopulations from the sub-regions (Figure 4C). The ensembles in each subpopulation during 20 min periods were then identified, and their averaged numbers were used to represent the rate of ensemble generation (Figure 4D). Consistent with the results that mapped all ensembles in the whole imaged fields (Figure 3G), XAV939 brains had a significantly increased average numbers of ensembles in the 100-neuron subpopulations (Figure 4E). Thus, the increased ensemble number in XAV939 mice was probably due to enhanced pairwise correlations (Figure 1J) and neuronal group coactivations (Figure 2H) rather than an artifact of simply imaging larger neuronal populations. Overall, our findings suggest that neuronal overproduction leads to the generation more functional ensembles.

XAV939 Treatment Enhances Functional Segregation of Ensembles

Because ensembles are likely built from enhanced synaptic connections among coactive neurons (Carrillo-Reid et al., 2016; Sanchez-Vives and McCormick, 2000), the similar functional preference of interconnected neurons (Ko et al., 2011; Lee et al., 2016) predicts that ensembles may be built with

functionally related neurons (Miller et al., 2014). Therefore, ensembles that overlap in constituent neurons could have functional similarity, and one may be able to assess functional integration or segregation of local neural networks by measuring the extent of ensemble overlapping. To this end, we constructed a binary matrix to denote constituent neurons of individual ensembles (Figure 5A), measured the fraction of ensemble pairs that shared neurons (Figure 5B), and quantified the level of overlapping by calculating cosine similarity of pairs of ensemble vectors (Figure 5C). In wild-type control animals, overlapped fractions of visually evoked ensembles were smaller than those of spontaneous ones (Figure 5B), but evoked ensembles exhibited higher average cosine similarity (Figure 5D), indicating stronger clustering in evoked ensembles. Compared to the control brains, ensemble overlapping occurred in smaller fractions of spontaneous and evoked ensembles in XAV939 brains (Figure 5B). Moreover, XAV939 brains exhibited stronger clustering of both spontaneous and evoked ensembles (Figure 5D).

To explore the link between ensemble clustering and functional segregation, we extracted high-activity frames corresponding to each orientated stimulus (Figure 5E), identified 4 groups of orientation-specific evoked ensembles (Figure 5F), and then calculated the cosine similarity between these ensembles (Figure 5F). Although orientation-specific evoked ensembles of the same groups were highly clustered, as shown by the large average cosine similarity, weak clustering was found across different groups (Figures 5F and 5G). Moreover, the ratio of intra- to intergroup clustering was larger than that calculated from surrogate datasets (Figure 5H), indicating that ensemble clustering was associated with functional separation. To validate this, we presented animals with vertical drifting gratings ($\theta = 90^\circ$), rotated the gratings by different angles ($\Delta\theta$ = 20°, 30°, or 90°), and then compared the clustering levels between groups of orientation-specific evoked ensembles (Figure 5I). The ratio of intra- to intergroup clustering increased with differences in orientation (Figure 5J), indicating that the extent of ensemble clustering reflected their functional segregation. Consistent with stronger ensemble clustering (Figures 5B and 5D), XAV939 brains showed higher ratios of intra- to intergroup overlapping of orientation-specific ensembles (Figures 5H and 5J). Thus, XAV939 treatment, which induces neuronal overproduction, also enhances clustering of ensembles and functional segregation of local neural networks.

XAV939 Treatment Improves Behavioral Orientation Discrimination

We finally assessed whether XAV939 treatment altered behavioral performance by comparing the orientation discrimination behavior of wild-type animals (n = 8 mice) and XAV939-engineered animals (n = 8 mice). Awake behaving mice were trained on an operant lick-left/lick-right task (Guo et al., 2014) in response to visual cues (drifting vertical or horizontal gratings) and rewarded or punished for correct or incorrect licks, respectively (Figures 6A and 6B; Movie S3). Control and XAV939-engineered animals gradually improved their performance on obtaining a water reward from both left and right licks over days at similar rates (Figures 6E, S3A, and S3D), indicating that potential behavioral deficits in XAV939 mice (Fang et al., 2014) did not influence orientation discrimination during the training phase. After the correct lick rate of each animal reached 80%, we rotated both gratings by the same angles ($\Delta\theta$ = 15°, 20°, or 25°) (Figure 6C). The range of rotation (15°–25°) was estimated from our intragroup/intergroup ratio of ensemble overlapping result (Figure 5J) and from previous studies that measured orientation discriminability of wild-type mice (Andermann et al., 2010; Lee et al., 2012). If mice were able to distinguish the new orientated gratings from the original ones, they were inclined to reject licking; therefore, the correct lick rates declined with increasing orientation deviation (Figures 6F, S3B, and S3E). Furthermore, when only the lick-left cue was rotated (Figure 6D), the rate of correct left licks was significantly reduced (Figure 6G), compared to that of correct right licks (Figures S3C and S3F). In addition, the capability of discriminating unchanged and rotated orientations (discriminability, d') (Andermann et al., 2010) increased with orientation deviation (Figure 6H). These results indicated that mice were able to discriminate a fine orientation difference (15°–20°) in these behavioral tasks.

XAV939 mice consistently outperformed their wild-type counterparts in detecting finer orientation changes, as shown by a higher reduction of correct lick rates in the two tasks and higher discriminability in task 2 (Figures 6F–6H). The better performance of XAV939 mice should not result from compulsive and repetitive behaviors (Fang et al., 2014), because this was not observed during the tasks (data not shown). Moreover, if XAV939 mice behaved repetitively, they would rather lick the spouts more frequently than reject licking. The marked behavioral difference between groups of wild-type and XAV939-treated mice indicates that XAV939-treated mice, which have more neurons in V1, also have better orientation discrimination capability.

DISCUSSION

Here, we find that a manipulation that increases neuronal number also increases functional modularity in the neocortex and perceptual discrimination. Although neurogenesis plays important roles in organizing microcircuitry (Li et al., 2012; Ohtsuki et al., 2012; Yu et al., 2009), a moderate change of neuronal number is often considered functionally insignificant, probably because programmed cell death of immature neurons and elimination of exuberant projections occur extensively during early brain development (Buss et al., 2006; Innocenti and Price, 2005). But our findings show that even a moderate increase (~18%) of neuronal production can substantially enhance the functional clustering of neuronal ensembles (Figure 5) and improves visual discriminability in adulthood (Figure 6). Thus, mild variations in early cortical developmental processes, such as neuronal production and migration, could affect future cortical function, at least in V1. Because circuit wiring principles are highly conserved among brains (Sterling and Laughlin, 2015), our results may have wider implications in the developmental basis of neural circuitry evolution and individuality. Given the denser neuronal packing in primates and varying neuronal density and number among human individuals, our findings can help explain the superior visual acuity in primates compared to nonprimates (Srinivasan et al., 2015) and the

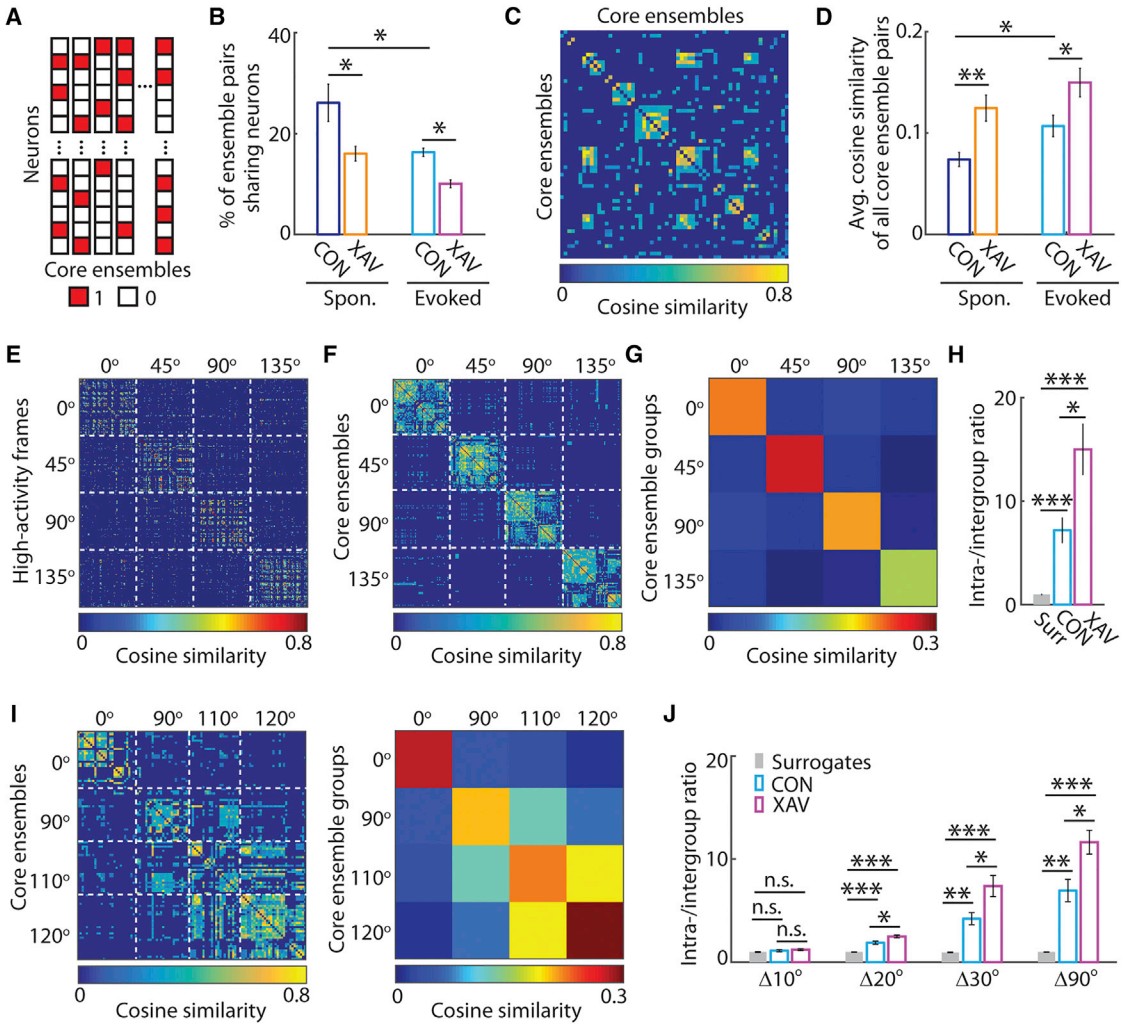

Figure 5. XAV939 Treatment Improves the Functional Segregation of Ensembles

(A) Schematic illustrating the constituent neurons of core ensembles. Some core ensembles overlap in constituent neurons.

(B) XAV939 treatment reduced the proportion of overlapping ensemble pairs. The proportion was smaller in evoked ensembles than in spontaneous ones.

(C) The levels of ensemble overlapping were calculated by the cosine similarity of ensemble vectors. Auto-correlation was set as 0.

(D) XAV939 treatment raised the level of ensemble overlapping. The average cosine similarity of all ensemble pairs was larger in evoked ensembles than in spontaneous ensembles.

(E) An example of clusters of high-activity frames corresponding to visual stimulation of each orientation. White dashed lines separate different groups of high-activity frames. The level of frame correlation was calculated by the cosine similarity of high-activity frame pairs.

(F) An example of the overlapping of orientation-specific evoked core ensembles. White dashed lines separate different groups of core ensembles. The level of ensemble overlapping was calculated by the cosine similarity of core ensemble pairs. Auto-overlapping was set as 0.

(G) Orientation-specific evoked ensembles exhibited high intragroup and low intergroup overlapping. The overlapping levels of orientation-specific ensemble groups were measured by the average cosine similarity of pairs of intra- or intergroup ensembles.

(H) XAV939 treatment elevated the ratio of intra- to intergroup overlapping of orientation-specific evoked ensembles. Surrogates (Surr) were randomized neuron groups in which constituent neurons of evoked ensembles were randomly exchanged, while the number and size of ensembles and the participation rate of each neuron in all ensembles were preserved.

(I) The extent of ensemble overlapping was associated with their functional similarity. Evoked ensembles of similar orientation preference exhibited higher levels of overlapping.

(J) The ratio of intra- to intergroup overlapping of evoked ensembles increased with the orientation difference. Increasing neuronal density significantly enlarged the ratios when the orientation difference was no smaller than 20°.

Data are represented as mean ± SEM; *p < 0.05, **p < 0.01, ***p < 0.001; n.s., not significant; Wilcoxon rank-sum test or Wilcoxon signed-rank test (Spon. versus Evoked of control in B and D).

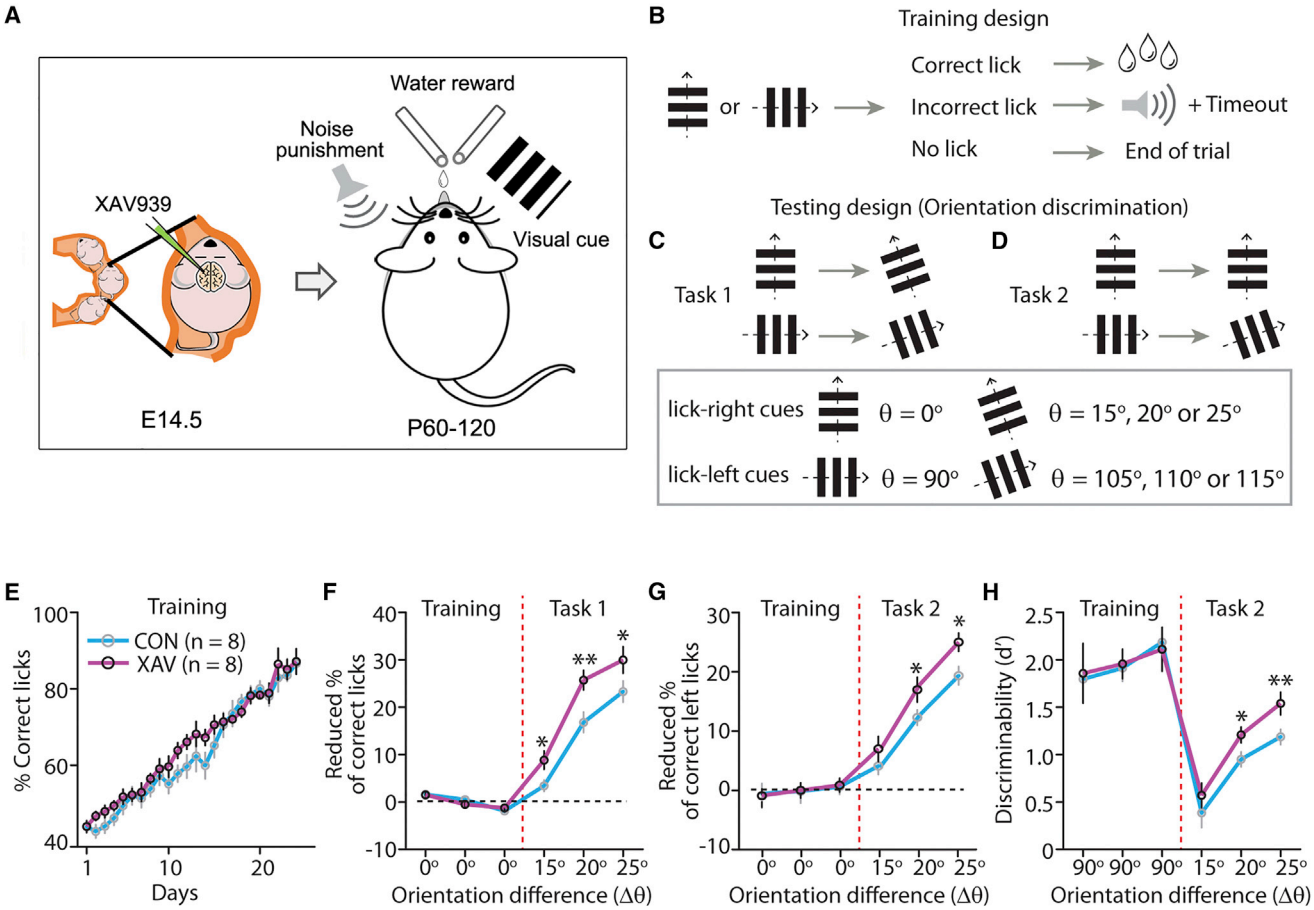

Figure 6. XAV939-Treated Mice Show Improved Orientation Discrimination

(A–D) Schematic illustrating the lick-left/lick-right behavior setup (A), the training design (B), and two tasks (C) and (D) for evaluating orientation discrimination of awake behaving mice (XAV939-treated mice, n = 8; control mice, n = 8).

(E) The rates of correct licks in response to visual cues gradually increased over days of training.

(F–H) XAV939-treated mice outperformed control mice in detecting finer orientation differences. The average correct rates in response to the original cues during the last 3 conservative training days were set as 0 (black dotted lines), and the relative correct rates in response to the rotated gratings were shown (F and G). The discriminability (*d'*) represented the capability of animals distinguishing gratings of different orientations (H). With the increase of orientation difference, reduction of correct rates (F and G) and discriminability increased (H).

Data are represented as mean ± SEM; *p < 0.05, **p < 0.01; Wilcoxon rank-sum test. See also Figure S3 and Movie S3.

individual differences of visual sensitivity among humans (Song et al., 2013). Furthermore, the correlation between increased number and clustering of ensembles and the improved behavioral performance of XAV939-engineered mice could help explain the increased cognitive capabilities of humans, because their extended neurogenesis period (Lui et al., 2011) could lead to increased number and clustering of neuronal ensembles.

Effect of Neuronal Production in Regulating Neuronal Ensembles

Because ensembles are stable groups of neurons (Figure 3E) (Carrillo-Reid et al., 2016; Miller et al., 2014), most observed ensembles are unlikely to be newly formed during the period of imaging and stimulation (~30 min), which was too short for neurons to reconfigure a considerable number of synapses (Yang et al., 2009). More plausible is that the observed ensembles were drawn from an intrinsic ensemble repertoire (lexicon or vocabulary) (Luczak et al., 2009; Miller et al., 2014), selected or imprinted by past cortical development or activity (Carrillo-Reid et al., 2016; Edelman, 1993). This common repertoire may be sampled widely by spontaneous events but specifically recruited by stimuli (Luczak et al., 2009; Miller et al., 2014), resulting in higher clustering of evoked ensembles than spontaneous ones (Figures 5B and 5D). We found that cortices with increased neuronal production exhibited similar orientation selectivity of individual neurons to wild-type cortices (Figure 1I), suggesting their ability in receiving visual inputs did not substantially differ. Therefore, the larger number of ensembles in XAV939 brains may result from an increase in the size and/or sampling or recruitment of this intrinsic ensemble repertoire, both of which probably emerge from changes of neuronal connectivity that could be

reflected by altered pairwise correlations (Figure 1J) and increased neuronal group coactivation (Figure 2H). In addition, the larger differences among ensembles in XAV939 animals could reflect a larger multidimensional space for the population dynamics to occupy.

Potential Circuit Mechanisms

We provide evidence that a manipulation of increasing neuronal numbers in the visual cortex also leads to increased neuronal ensembles and perceptual discrimination, but the exact mechanisms are not elucidated in the present study. Although XAV939 injections likely have many effects on the circuit, we suspect that neuronal overproduction could be the main reason that XAV939 injections alter functional circuits. Because neuronal overproduction did not substantially affect the spiking rates (Figure 1H) or functional properties of individual neurons, e.g., orientation selectivity (Figure 1I), the altered ensemble number may be due to changes in the correlated activation of neurons. As reported, XAV939 injections lead to a higher density of mature spines and higher amplitude of spontaneous excitatory postsynaptic currents (Fang et al., 2014), both of which could reflect stronger synaptic connectivity. Because the strength of synaptic connections mirrors the pairwise correlation and orientation tuning similarity of neurons (Cossell et al., 2015; Ko et al., 2011; Lee et al., 2016), neuronal overproduction might therefore increase ensemble number by increasing synaptic connection and strength. Moreover, after XAV939 injections, more interneurons are recruited to layer 2/3 and stronger spontaneous inhibitory postsynaptic currents are found in layer 2/3 excitatory neurons (Fang et al., 2014). This elevated inhibition could enhance the synchronization of connected neurons (Bush and Sejnowski, 1996) and secondarily increase the number of ensembles, by orthogonalizing and separating them in a multidimensional space (Agetsuma et al., 2017) (Figure 3E). In addition to alterations in synaptic connections and inhibition of local networks, global factors, such as astrocytes (Poskanzer and Yuste, 2011, 2016) or internal brain states (Poulet and Petersen, 2008), that modulate neuronal correlation and synchrony may indirectly contribute to the increased ensemble number in neuron-overproduced brains. Although we did not dissect the potential contributions of each possible factor in the regulation of ensemble number, based on our evidence, we favor the hypothesis that neuronal overproduction could be a starting point to induce the various anatomical and physiological alterations that eventually generate more ensembles.

Link between Neuronal Ensemble Organization and Behavior

Finally, neuronal ensemble activity and reactivation in different brain regions have been linked to behaviors, such as memory and decision-making tasks (Cai et al., 2016; Liu et al., 2012; Malvache et al., 2016; Siniscalchi et al., 2016; Zagha et al., 2015). Yet it is unclear how alteration of ensemble organization influences or reflects the changes of behavioral preference and consistency. Although we did not directly show that altering ensemble organization elicits behavioral changes, we favor the hypothesis that ensemble organization in V1 is functionally linked to orientation discrimination behavior for 3 reasons. First, ensemble clustering is associated with functional segregation of orientation preference (Figure 5). Second, ensemble clustering (Figure 5J) and orientation discriminability (Figure 6H) both increase with orientation difference in a visual stimulation task. Third, the same manipulation (neuronal production) concomitantly increases ensemble clustering (Figure 5) and improves orientation discriminability (Figures 6F–6H) in XAV939-engineered mice. Our findings collectively raise the challenge to elucidate the causation between activity of emergent functional states of neural circuits, such as ensembles, and behavior.

EXPERIMENTAL PROCEDURES

Further details and an outline of resources used in this work can be found in Supplemental Experimental Procedures.

Animals

All experimental procedures were approved and carried out in accordance with Columbia University institutional animal care guidelines. Imaging and behavioral experiments were conducted on naive (not exposed to any experiment or training) CD-1 mice of both sexes age P40–P120.

Visual Stimulation

Visual stimuli were generated using the MATLAB Psychophysics Toolbox (MathWorks) and displayed on a liquid crystal display (LCD) monitor (19 inches, 60 Hz refresh rate, Dell) positioned 15 cm from the right eye, roughly at 45° to the long axis of the animal. Sinusoidal gratings (100% contrast, 0.035 cycles per degree, 2 cycles/s) drifting in 8 directions in random orders were presented for 4 s, followed by 4 s of mean luminescence gray screen (15–20 repetitions). The sequences of gratings played in MATLAB were synchronized with image acquisition using the Sutter software (Mscan, Sutter Instrument).

Orientation Discrimination Behavioral Test

After attaching a titanium head plate to the skull, the mice were allowed to recover for 3 days in their home cages and get accustomed to experimenter handling. They were then water deprived during the entire experiment. The entire experiment consisted of three phases—habituation (1–2 weeks), training (3–5 weeks), and testing (1 week)—and was conducted in a black box to preclude environmental interference. Visual stimulation and paired reward and punishment were automatically controlled by custom-written MATLAB (MathWorks) and Arduino IDE (Arduino) codes.

Two-Photon Calcium Imaging

Before imaging, the cranial window was sealed with 1.5%–1.6% agarose and then secured by a glass coverslip. At the time of imaging, light anesthesia (body temperature of ~37.5°C, heart rate of 430–480 beats/min, respiration rate of 90–110 breaths/min, and oxygen saturation of 97.5%) was maintained by isoflurane (0.8%–1%). The activity of cortical neurons was monitored by imaging fluorescence with a two-photon microscope (Moveable Objective Microscope, Sutter Instrument) and a mode-locked dispersion-precompensated Ti:Sapphire laser (Chameleon Vision II, Coherent) at 880 nm (for OGB1), 940 nm (for GCaMP6s), or 1,040 nm (for Sulforhodamine 101) through a 20× (0.95 numerical aperture [NA], Olympus) or 25× (1.05 NA, Olympus) water immersion objective. The fluorescence signal was detected with a photomultiplier tube (PMT, Hamamatsu), followed by a low-noise amplifier (Stanford Research Systems). Scanning and image acquisition were controlled by Sutter software (4.07 frames/s for 512 × 512 pixels, Mscan, Sutter Instrument).

Neuronal Counts

Neuronal counts were assessed blindly to the phenotype of the animals with automatic software algorithms (Caltracer 2.0) that identified each cell body, using the same parameters for both XAV939-treated and control animals. Neuronal density was measured by counting the number of OGB1-positive neurons in 250 × 250 μm^2 regions.

Analysis of Orientation Selectivity and Preference

The responses (ΔF/F) to each grating stimulus from 15 to 20 trials were averaged to obtain orientation tuning curves (polar plots). Orientation selectivity was $1 - CV = \left|\sum_k R_k \cdot exp(2i\theta_k)/\sum_k R_k\right|$ and direction selectivity was $1 -$ direction circular variance (DCV) $= \left|\sum_k R_k \cdot exp(i\theta_k)/\sum_k R_k\right|$, where CV is the circular variance, R_k is the response to each orientation (k = 1–8), i is the imaginary unit, and θ_k is the orientation angle in radians $(k-1)\pi/4$. Neurons with OSI $\geq$ 0.2 were determined to be orientation selective. Their preferred orientation was determined as the orientation that invoked the highest response.

Core Ensemble Identification

Neuronal ensembles were generally considered to be groups of neurons recurrently exhibiting synchronous and/or sequential coherent activity patterns. In this study, we searched for sets of common neurons ($\geq$3 neurons) that were repeatedly coactive in $\geq$3 mutually correlated high-activity frames. To identify orientation-specific evoked ensembles, we extracted 4 groups of frames that corresponded to each oriented grating stimulation and used the same ensemble searching and filtering algorithm for each group of frames.

Statistical Analysis

To determine statistical significances, we used Student's t test for comparing neuronal densities of 2 groups of mice (control versus XAV939), nonparametric Wilcoxon rank-sum test for values of non-Gaussian distributions (e.g., spiking rates, pairwise correlation coefficients, ensemble numbers, and overlapping ratios) of 2 groups of mice (control versus XAV939) or between observed and surrogate datasets, and nonparametric Wilcoxon signed-rank test paired values of 2 conditions of the same group of mice (spontaneous versus evoked). Statistical tests were performed with MATLAB (MathWorks). All data in bar graphs represent mean ± SEM unless otherwise indicated. The level of significance was set at $p < 0.05$.

SUPPLEMENTAL INFORMATION

Supplemental Information includes Supplemental Experimental Procedures, three figures, and three movies and can be found with this article online at https://doi.org/10.1016/j.celrep.2017.09.040.

AUTHOR CONTRIBUTIONS

W.-Q.F. and R.Y. designed the study, W.-Q.F. conducted the experiments and analyzed the data, and W.-Q.F. and R.Y. wrote the manuscript.

ACKNOWLEDGMENTS

We thank Weijian Yang, Shuting Han, and other laboratory members for discussions and comments. We also thank Yeonsook Shin, Reka Letso, and Mari Bando for virus injection; Olga Yarygina for behavioral training; and Jae-eun Miller for the behavior setup. This work was supported by the NEI (DP1EY024503 and R01EY011787), NIMH (R01MH101218 and R01MH100561) and DARPA SIMPLEX N66001-15-C-4032. This material is based upon work supported by, or partly by, the U.S. Army Research Laboratory and the U.S. Army Research Office under contract W911NF-12-1-0594 (MURI).

Received: July 28, 2017
Revised: September 2, 2017
Accepted: September 11, 2017
Published: October 10, 2017

REFERENCES

Agetsuma, M., Hamm, J.P., Sato, I., and Yuste, R. (2017). Parvalbumin-positive interneurons regulate neuronal ensembles in visual cortex. Cerebral Cortex, Published online July 6, 2017. https://doi.org/10.1093/cercor/bhx169.

Andermann, M.L., Kerlin, A.M., and Reid, R.C. (2010). Chronic cellular imaging of mouse visual cortex during operant behavior and passive viewing. Front. Cell. Neurosci. *4*, 3.

Averbeck, B.B., Latham, P.E., and Pouget, A. (2006). Neural correlations, population coding and computation. Nat. Rev. Neurosci. *7*, 358–366.

Bush, P., and Sejnowski, T. (1996). Inhibition synchronizes sparsely connected cortical neurons within and between columns in realistic network models. J Comput Neurosci. *3*, 91–110.

Buss, R.R., Sun, W., and Oppenheim, R.W. (2006). Adaptive roles of programmed cell death during nervous system development. Annu. Rev. Neurosci. *29*, 1–35.

Cai, D.J., Aharoni, D., Shuman, T., Shobe, J., Biane, J., Song, W., Wei, B., Veshkini, M., La-Vu, M., Lou, J., et al. (2016). A shared neural ensemble links distinct contextual memories encoded close in time. Nature *534*, 115–118.

Carrillo-Reid, L., Yang, W., Bando, Y., Peterka, D.S., and Yuste, R. (2016). Imprinting and recalling cortical ensembles. Science *353*, 691–694.

Chen, T.W., Wardill, T.J., Sun, Y., Pulver, S.R., Renninger, S.L., Baohan, A., Schreiter, E.R., Kerr, R.A., Orger, M.B., Jayaraman, V., et al. (2013). Ultrasensitive fluorescent proteins for imaging neuronal activity. Nature *499*, 295–300.

Collins, C.E., Airey, D.C., Young, N.A., Leitch, D.B., and Kaas, J.H. (2010). Neuron densities vary across and within cortical areas in primates. Proc. Natl. Acad. Sci. USA *107*, 15927–15932.

Cossart, R., Aronov, D., and Yuste, R. (2003). Attractor dynamics of network UP states in the neocortex. Nature *423*, 283–288.

Cossell, L., Iacaruso, M.F., Muir, D.R., Houlton, R., Sader, E.N., Ko, H., Hofer, S.B., and Mrsic-Flogel, T.D. (2015). Functional organization of excitatory synaptic strength in primary visual cortex. Nature *518*, 399–403.

Edelman, G.M. (1993). Neural Darwinism: selection and reentrant signaling in higher brain function. Neuron *10*, 115–125.

Fang, W.Q., Chen, W.W., Fu, A.K., and Ip, N.Y. (2013). Axin directs the amplification and differentiation of intermediate progenitors in the developing cerebral cortex. Neuron *79*, 665–679.

Fang, W.Q., Chen, W.W., Jiang, L., Liu, K., Yung, W.H., Fu, A.K., and Ip, N.Y. (2014). Overproduction of upper-layer neurons in the neocortex leads to autism-like features in mice. Cell Rep. *9*, 1635–1643.

Feldt Muldoon, S., Soltesz, I., and Cossart, R. (2013). Spatially clustered neuronal assemblies comprise the microstructure of synchrony in chronically epileptic networks. Proc. Natl. Acad. Sci. USA *110*, 3567–3572.

Guo, Z.V., Hires, S.A., Li, N., O'Connor, D.H., Komiyama, T., Ophir, E., Huber, D., Bonardi, C., Morandell, K., Gutnisky, D., et al. (2014). Procedures for behavioral experiments in head-fixed mice. PLoS ONE *9*, e88678.

Harris, K.D. (2005). Neural signatures of cell assembly organization. Nat. Rev. Neurosci. *6*, 399–407.

Harris, K.D., Csicsvari, J., Hirase, H., Dragoi, G., and Buzsáki, G. (2003). Organization of cell assemblies in the hippocampus. Nature *424*, 552–556.

Hebb, D.O. (1949). The organization of behavior; a neuropsychological theory (Wiley).

Herculano-Houzel, S. (2009). The human brain in numbers: a linearly scaled-up primate brain. Front. Hum. Neurosci. *3*, 31.

Herculano-Houzel, S., Manger, P.R., and Kaas, J.H. (2014). Brain scaling in mammalian evolution as a consequence of concerted and mosaic changes in numbers of neurons and average neuronal cell size. Front. Neuroanat. *8*, 77.

Hubel, D.H., and Wiesel, T.N. (1959). Receptive fields of single neurones in the cat's striate cortex. J. Physiol. *148*, 574–591.

Ikegaya, Y., Aaron, G., Cossart, R., Aronov, D., Lampl, I., Ferster, D., and Yuste, R. (2004). Synfire chains and cortical songs: temporal modules of cortical activity. Science *304*, 559–564.

Innocenti, G.M., and Price, D.J. (2005). Exuberance in the development of cortical networks. Nat. Rev. Neurosci. *6*, 955–965.

Kenet, T., Bibitchkov, D., Tsodyks, M., Grinvald, A., and Arieli, A. (2003). Spontaneously emerging cortical representations of visual attributes. Nature *425*, 954–956.

Ko, H., Hofer, S.B., Pichler, B., Buchanan, K.A., Sjöström, P.J., and Mrsic-Flogel, T.D. (2011). Functional specificity of local synaptic connections in neocortical networks. Nature *473*, 87–91.

Lampl, I., Reichova, I., and Ferster, D. (1999). Synchronous membrane potential fluctuations in neurons of the cat visual cortex. Neuron *22*, 361–374.

Lee, S.H., Kwan, A.C., Zhang, S., Phoumthipphavong, V., Flannery, J.G., Masmanidis, S.C., Taniguchi, H., Huang, Z.J., Zhang, F., Boyden, E.S., et al. (2012). Activation of specific interneurons improves V1 feature selectivity and visual perception. Nature *488*, 379–383.

Lee, W.C., Bonin, V., Reed, M., Graham, B.J., Hood, G., Glattfelder, K., and Reid, R.C. (2016). Anatomy and function of an excitatory network in the visual cortex. Nature *532*, 370–374.

Li, Y., Lu, H., Cheng, P.L., Ge, S., Xu, H., Shi, S.H., and Dan, Y. (2012). Clonally related visual cortical neurons show similar stimulus feature selectivity. Nature *486*, 118–121.

Liu, X., Ramirez, S., Pang, P.T., Puryear, C.B., Govindarajan, A., Deisseroth, K., and Tonegawa, S. (2012). Optogenetic stimulation of a hippocampal engram activates fear memory recall. Nature *484*, 381–385.

Luczak, A., Barthó, P., and Harris, K.D. (2009). Spontaneous events outline the realm of possible sensory responses in neocortical populations. Neuron *62*, 413–425.

Lui, J.H., Hansen, D.V., and Kriegstein, A.R. (2011). Development and evolution of the human neocortex. Cell *146*, 18–36.

MacLean, J.N., Watson, B.O., Aaron, G.B., and Yuste, R. (2005). Internal dynamics determine the cortical response to thalamic stimulation. Neuron *48*, 811–823.

Malvache, A., Reichinnek, S., Villette, V., Haimerl, C., and Cossart, R. (2016). Awake hippocampal reactivations project onto orthogonal neuronal assemblies. Science *353*, 1280–1283.

Miller, J.E., Ayzenshtat, I., Carrillo-Reid, L., and Yuste, R. (2014). Visual stimuli recruit intrinsically generated cortical ensembles. Proc. Natl. Acad. Sci. USA *111*, E4053–E4061.

Mueller, S., Wang, D., Fox, M.D., Yeo, B.T., Sepulcre, J., Sabuncu, M.R., Shafee, R., Lu, J., and Liu, H. (2013). Individual variability in functional connectivity architecture of the human brain. Neuron *77*, 586–595.

Ohtsuki, G., Nishiyama, M., Yoshida, T., Murakami, T., Histed, M., Lois, C., and Ohki, K. (2012). Similarity of visual selectivity among clonally related neurons in visual cortex. Neuron *75*, 65–72.

Olkowicz, S., Kocourek, M., Lučan, R.K., Porteš, M., Fitch, W.T., Herculano-Houzel, S., and Němec, P. (2016). Birds have primate-like numbers of neurons in the forebrain. Proc. Natl. Acad. Sci. USA *113*, 7255–7260.

Pnevmatikakis, E.A., Soudry, D., Gao, Y., Machado, T.A., Merel, J., Pfau, D., Reardon, T., Mu, Y., Lacefield, C., Yang, W., et al. (2016). Simultaneous denoising, deconvolution, and demixing of calcium imaging data. Neuron *89*, 285–299.

Poskanzer, K.E., and Yuste, R. (2011). Astrocytic regulation of cortical UP states. Proc. Natl. Acad. Sci. USA *108*, 18453–18458.

Poskanzer, K.E., and Yuste, R. (2016). Astrocytes regulate cortical state switching in vivo. Proc. Natl. Acad. Sci. USA *113*, E2675–E2684.

Poulet, J.F., and Petersen, C.C. (2008). Internal brain state regulates membrane potential synchrony in barrel cortex of behaving mice. Nature *454*, 881–885.

Roth, G., and Dicke, U. (2005). Evolution of the brain and intelligence. Trends Cogn. Sci. *9*, 250–257.

Sanchez-Vives, M.V., and McCormick, D.A. (2000). Cellular and network mechanisms of rhythmic recurrent activity in neocortex. Nat. Neurosci. *3*, 1027–1034.

Schneidman, E., Berry, M.J., 2nd, Segev, R., and Bialek, W. (2006). Weak pairwise correlations imply strongly correlated network states in a neural population. Nature *440*, 1007–1012.

Siniscalchi, M.J., Phoumthipphavong, V., Ali, F., Lozano, M., and Kwan, A.C. (2016). Fast and slow transitions in frontal ensemble activity during flexible sensorimotor behavior. Nat. Neurosci. *19*, 1234–1242.

Song, C., Schwarzkopf, D.S., and Rees, G. (2013). Variability in visual cortex size reflects tradeoff between local orientation sensitivity and global orientation modulation. Nat. Commun. *4*, 2201.

Srinivasan, S., Carlo, C.N., and Stevens, C.F. (2015). Predicting visual acuity from the structure of visual cortex. Proc. Natl. Acad. Sci. USA *112*, 7815–7820.

Sterling, P., and Laughlin, S. (2015). Principles of neural design (MIT Press).

Stosiek, C., Garaschuk, O., Holthoff, K., and Konnerth, A. (2003). In vivo two-photon calcium imaging of neuronal networks. Proc. Natl. Acad. Sci. USA *100*, 7319–7324.

Vogel, E.K., and Machizawa, M.G. (2004). Neural activity predicts individual differences in visual working memory capacity. Nature *428*, 748–751.

Ward, B.C., Nordeen, E.J., and Nordeen, K.W. (1998). Individual variation in neuron number predicts differences in the propensity for avian vocal imitation. Proc. Natl. Acad. Sci. USA *95*, 1277–1282.

White, L.E., and Fitzpatrick, D. (2007). Vision and cortical map development. Neuron *56*, 327–338.

Williams, R.W., and Herrup, K. (1988). The control of neuron number. Annu. Rev. Neurosci. *11*, 423–453.

Yang, G., Pan, F., and Gan, W.B. (2009). Stably maintained dendritic spines are associated with lifelong memories. Nature *462*, 920–924.

Yang, W., Miller, J.E., Carrillo-Reid, L., Pnevmatikakis, E., Paninski, L., Yuste, R., and Peterka, D.S. (2016). Simultaneous multi-plane imaging of neural circuits. Neuron *89*, 269–284.

Yu, Y.C., Bultje, R.S., Wang, X., and Shi, S.H. (2009). Specific synapses develop preferentially among sister excitatory neurons in the neocortex. Nature *458*, 501–504.

Yuste, R. (2015). From the neuron doctrine to neural networks. Nat. Rev. Neurosci. *16*, 487–497.

Yuste, R., and Katz, L.C. (1991). Control of postsynaptic Ca2+ influx in developing neocortex by excitatory and inhibitory neurotransmitters. Neuron *6*, 333–344.

Zagha, E., Ge, X., and McCormick, D.A. (2015). Competing neural ensembles in motor cortex gate goal-directed motor output. Neuron *88*, 565–577.